# Effect of Matte-Sn Electroplating Parameters on the Thermomechanical Reliability of Lead-free Solder Joints

# Abhilaash Ajith Kumar and Werner Hügel, Ph.D.

Robert Bosch GmbH Schwieberdingen, Germany

#### **ABSTRACT**

The Most of the Cu/Cu alloy lead-frames of electronic components used for automotive applications contain electroplated matte-Sn terminal finish to improve the wettability of Sn-based Pbfree solders during reflow soldering process. When the solder joints are subjected to combined thermal and mechanical cyclic loading, the influence of matte-Sn electroplating parameters can lead to early and brittle failure of the solder joint. To test this hypothesis, a factorial design of experiments (DOE) has been conducted with LFPAK-MOSFET (hereafter referred to as LFPAK) components plated with different matte-Sn electroplating parameters and reflow soldered with two solder alloys (SAC 305 and Innolot). The LFPAK solder joints were then subjected to thermo-mechanical in-phase cyclic loading under different strain amplitudes. No electrical measurement is done to eradicate the effect of electrical current on the solder joint. The response to the DOE is the crack percentage obtained in the LFPAK solder joints after 1000 and 2000 cycles. The Innolot solder joints exhibited lower crack percentages than the SAC 305. The level of organic additives in the electroplating process of matte-Sn influences the failure mode of the solder joint. Microstructural investigation attributes the nature of failure to the morphology of the (Cu,Ni), Sn, IMC phase that forms on the component side of the solder joint.

Key words: Electroplating, Innolot, Intermetallics, Lead-free Solders, LFPAK, Matte-Sn, Mechanical Cycling, SAC, Thermal Cycling.

#### INTRODUCTION

A fundamental understanding of the various factors affecting the reliability of Pb-free solder joints under cyclic thermal and mechanical loads is required for automotive applications. Electronic components such as LFPAK-MOSFETs (LFPAK) with gull-wing shaped pins are commonly used in automotive applications where the solder joints are subjected to both thermal and mechanical strains during service. The combined loading increases the sensitivity of the processing parameters to early fatigue failures. Several studies on solder joint reliability were performed under pure thermal or pure mechanical cyclic loading [1]–[4]. Only few studies

have been conducted where both thermal and mechanical loading were simultaneously applied [5]–[7]. This study analyzes the impact of electroplating parameters of matte-Sn terminal finish on the thermo-mechanical reliability of LFPAK solder joints.

#### **EXPERIMENTAL**

In this study, the Cu lead-frames of the LFPAK components were coated with a Ni-underlayer (1-3  $\mu$ m) to eliminate the effect of alloying elements in the Cu lead-frames on the type and growth of the intermetallic (IMC) phase that grows on the interface. The LFPAK lead-frames were then subjected to matte-Sn electroplating process according to the parameters provided in table 1.

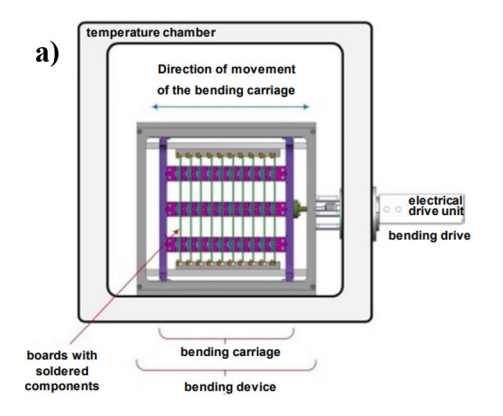
Table 1: Matte-Sn electroplating parameters for LFPAK lead-frames with Ni underlayer.

Matte-Sn plating variant	Temperature (°C)	Current Density (A/dm²)	Organic Conc. (mL/L)
N	22	15	2
V3	17.5	20	2
V9	17.5	20	10
V27	27.8	20	10

The plating variant N represents the nominal electroplating parameters used under standard industrial conditions and V3, V9, V27 represent parameters at the tolerance limits in the electroplating process. The time of electroplating process was adjusted to obtain a matte-Sn coating of 10  $\mu$ m. The matte-Sn thickness after electroplating was measured between 7-15 $\mu$ m in optical microscopy. The lead-frames were then bent and trimmed to obtain the LFPAK gull wing shape.

The LFPAK components were populated in 16 columns onto PCB test boards and reflow soldered using SAC305 or Innolot (Ag: 3.6, Cu: 0.6, Ni: 0.1, Sb: 1.3, Bi: 2.8 and remaining Sn) solder alloys. The reflow was done under similar conditions for both solder alloys with a ramp-soak-peak profile with maximum temperature of 260°C and time above liquidus (TAL) of 90s. The soldered PCB boards were placed with the top and bottom edges fixed

inside a bending vehicle consisting of a programmable electrical drive that imparts specified bending strains to the middle of the PCB boards. The bending vehicle is situated inside a temperaturecontrolled chamber as shown in figure 1a. The populated boards were subjected to 3-point in-phase bending and thermal cycling between 125°C/-40°C for 1000 and 2000 cycles. The load was applied at the center of the PCB (maximum microstrain of 1000/-600 ppm) which allowed the solder joints to experience 8 different levels of strain amplitude for the same thermal profile depending on the distance from the center of the PCB. A schematic of the in-phase thermo-mechanical bending test is shown in figure 1b. The individual LFPAK components were placed 0° with respect to bending direction. No electrical measurement was done to eradicate the effect of electrical current on the solder joint. The details of the experimental procedure are explained in [6]. In this study, the eight microstrain levels were reduced to 4 microstrain sets as seen in table 2 due to the negligible difference in solder joint performance and to improve the statistical accuracy during analysis.





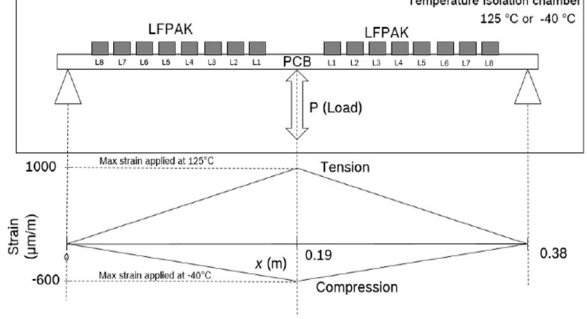


Figure 1: a) Schematic of the experimental bending vehicle used for in-phase thermo-mechanical bending test. b) Schematic showing the bending strain variation during tension and compression cycles.

After the specified number of cycles (1000 and 2000 cycles), the PCB boards with LFPAK components were taken out and subjected to metallographic processing and optical microscopy to obtain 2D cross sectional views of the solder joints. Figure 2a shows an example of a 2D cross section of a LFPAK solder joint after 2000 cycles. Figure 2b shows the schematic of LFPAK solder joint cross-section containing two cracks and the definitions of crack lengths and solder joint length. The total crack length (crack 1 length + crack 2 length + ....(if any)) present in the solder joint were divided by the solder joint length to obtain the crack %. To reduce the error in approximating 3D crack surface to a 2D crosssection plane, the crack % were measured for minimum 5 samples with same experimental conditions and the average crack % and standard deviations were calculated. Scanning electron microscopy (SEM) and energy dispersive X-ray spectroscopy (EDS) were done to investigate the microstructure and composition of the phases present at the interface.

Table 2: Tensile at 125°C and compressive at -40°C (indicated by - sign) microstrains ( $\mu\epsilon$ ) experienced by the LFPAK solder joints at eight microstrain levels (L1-L8). Eight microstrain levels were reduced to four microstrain sets and the corresponding average strain amplitude ( $\epsilon$ <sub>a</sub>) was calculated for each set.

με set	με levels	με applied at 125°C (ppm)	με applied at -40°C (ppm)	Strain amplitude εa= Δ(με)/2 (ppm)	Average εa per set (ppm)
1	L1	896.6	-541.2	718.9	678.3
	L2	793.1	-482.4	637.7	
2	L3	689.7	-423.5	556.6	516.0
	L4	586.2	-364.7	475.5	
3	L5	482.8	-305.9	394.3	353.8
	L6	379.3	-247.1	313.2	
4	L7	275.9	-188.2	232.0	191.5
	L8	172.4	-129.4	150.9	



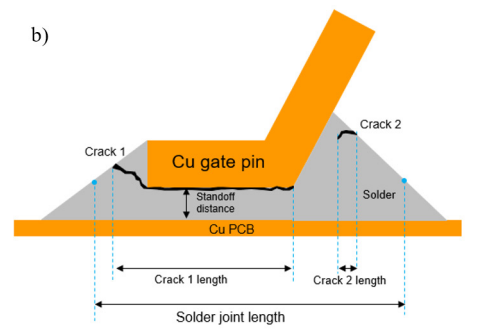


Figure 2: a) 2D cross sectional view of the LFPAK gull wing solder joint after 2000 cycles, b) Schematic of LFPAK cross-section containing two cracks showing the definitions of crack lengths and solder joint length.

# **RESULTS AND DISCUSSION**

Statistical analysis of LFPAK solder joints after 1000 and 2000 thermo-mechanical fatigue cycles

After thermo-mechanical cycling for 1000 and 2000 cycles, the crack percentage values were calculated for the LFPAK solder joints. The crack percentage values were subjected to pareto analysis to find the significance of each factor used in this study: A) Strain amplitude , B) Solder alloy, C) Electroplating parameter and D) Number of fatigue cycles.

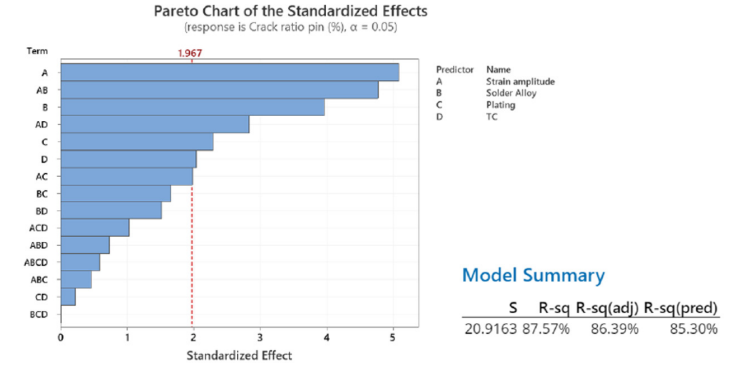
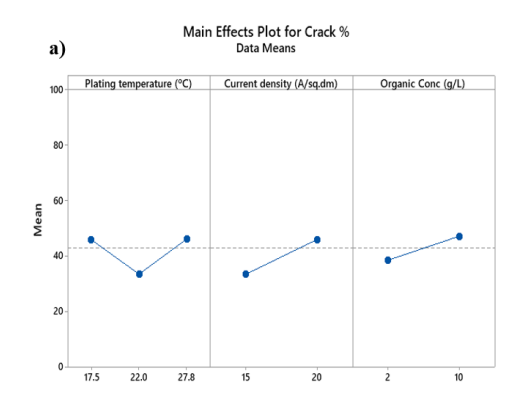
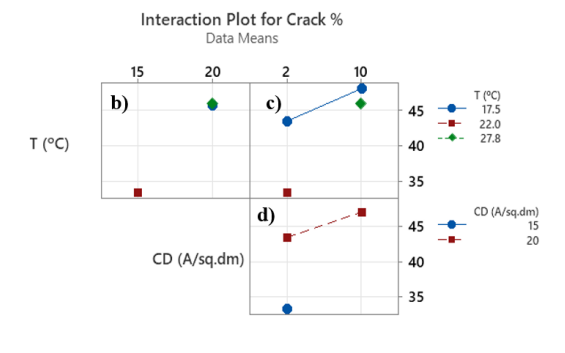


Figure 3: Pareto plot of crack percentage showing statistically significant main factors and interaction factors

The strain amplitude is taken as the continuous predictor and the order of significance of each factor and their interaction effects can

be seen in figure 3. The Pareto chart uses a standardized effects chart calculated using t-statistic to help visualize relative significance of each factor and its interactions. A reference line which was calculated based on the chosen confidence interval (95%) helps distinguish the most significant factors. In terms of main effects, the applied microstrain (A) has the highest impact followed by type of solder alloy (B), matte-Sn electroplating parameter (C) and no. of fatigue cycles (D) respectively. With respect to interaction effects, the AB interaction effect is the most significant followed by AD and AC. Higher order parameters are not statistically significant and can be ignored. Goodness of mode l fit is shown by the higher values of both R-sq and R-sq(pred) values.





Organic Conc (g/L)

Figure 4: a) Main effects plot showing the influence of individual electroplating parameters on the mean crack percentage. b)-d) Interaction plot of crack% showing the interaction effects of the electroplating parameters: plating temperature (T), current density (CD) and organic concentration (g/L).

The main effects shown in figure 4a provides information on the influence of individual electroplating parameters on the mean crack percentage. Plating temperature does not have a direct relationship with obtained crack percentages. There is a narrow process window around 22°C with respect to plating temperature which can provide good thermo-mechanical performance. With respect to current density, there is an increase in mean crack percentage irrespective of other plating parameters. Higher current densities

can increase the impurity levels in the plating which decreases the thermo-mechanical performance. The organic concentration in the electrolyte during plating also has direct relationship to mean crack percentages. But the influence of individual factors is not straightforward as combinations of these factors results in varied performance. Figure 4b-4d shows the interaction plot which captures the interaction between various electroplating parameters. Figure 4b shows the dependence of crack percentage on plating temperature (T) and current density (CD) at constant organic concentration in the electrolyte. As the current density increases to 20 A/dm<sup>2</sup>, average crack percentage is increased by almost same magnitude irrespective of whether the plating temperature was lowered to 17.5°C or increased to 27.8°C. In figure 4c, the effect of increasing the organic concentration is shown at various temperatures. At the organic concentration level of 2g/L (N and V3), the average crack percentage increased by a large magnitude as the temperature decreased from 22°C to 17.5°C. At the organic concentration level of 10g/L (V9 and V27), the mean crack percentage is lowered as the temperature increased from 17.5°C to 27.8°C. Figure 4d depicts that the mean crack percentage increases as the organic concentration in the electrolyte increases at higher constant current density of 20 A/dm<sup>2</sup>. Thus, increasing the organic content in the electrolyte decreases the thermo-mechanical performance irrespective of plating temperature and current density. Due to the interaction of all three plating parameters, it is pertinent to further discuss the results of the thermo-mechanical test in terms of the plating variants (N, V3, V9, V27) instead of individual plating parameters.

The mean crack percentage of each plating variant is plotted as a function of strain amplitude for SAC305 and Innolot (IL) solder alloys after 1000 and 2000 cycles in figure 5. The error bar originates from the nature of cross section which shows just one plane of a 3D crack surface. Below a threshold strain amplitude of 250 ppm, the crack percentages obtained between the different plating conditions (N, V3, V9, V27) is negligible or close to zero for both SAC305 and Innolot solder joints. This implies that if the LFPAK components were tested with a pure temperature cycle test, the effects of plating parameters and/or type of solder alloy cannot be distinguished within the test limits of 2000 cycles. Therefore, the difference in the crack percentage obtained at an early stage (<2000 cycles) arises from the combination of thermal and applied strain contributions.

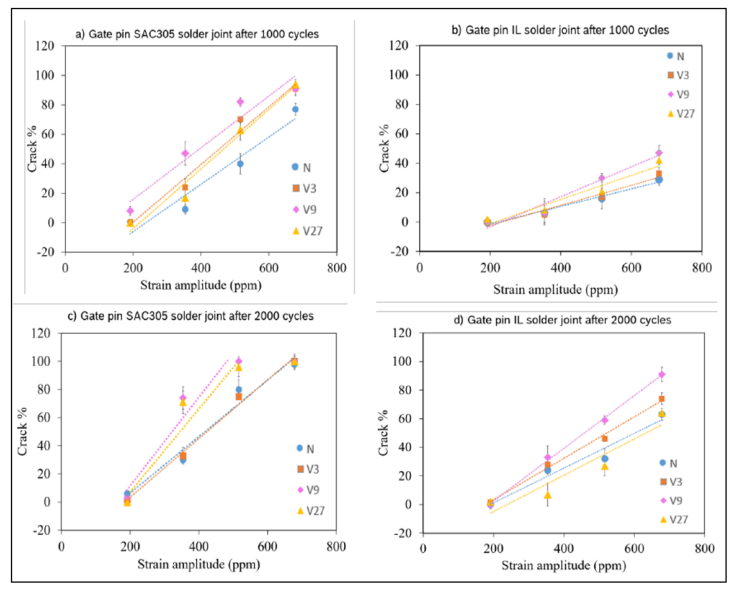


Figure 5: Strain amplitude vs crack percentage with various matte-Sn plating parameters: a) SAC305 soldered LFPAK after 1000 cycles, b) Innolot (IL) soldered LFPAK after 1000 cycles, c) SAC305 soldered LFPAK after 2000 cycles, d) Innolot soldered LFPAK after 2000 cycles. Note here that the crack percentage values are physically bound between 0% and 100%.

Comparing the solder alloy performance, the Innolot solder joints show very low crack percentage values than SAC305 solder joints after both 1000 and 2000 cycles for the same strain amplitude. The Innolot solder joints did not fail to 100% even at the maximum applied strain after 1000 cycles whereas the SAC solder joints started showing complete failure at the maximum applied strain after 1000 cycles. After 2000 cycles, 100% crack propagation occurred in Innolot solder joints which experienced the maximum strain amplitude. In comparison, the SAC solder joints showed complete failure at 516 ppm strain amplitude. The difference in reliability performance between SAC and Innolot solder joints pertains to the higher creep resistance of the Innolot solder alloy compared to the SAC305 solder alloy because of the combined effect of solid solution strengthening and enhanced precipitation hardening with large concentration of IMC precipitates in the solder matrix [8].

Considering the plating variants, the LFPAK solder joints plated with parameter N showed the lowest crack percentage whereas the solder joints with parameter V9 showed the highest crack percentage values for both SAC305 and Innolot after 1000 cycles. After 2000 cycles, all the plating variants in SAC solder joints showed 100% crack propagation at 516 ppm and 678.3 ppm strain amplitudes. At 353 ppm, V9 and V27 (plated with higher organic concentration) in the electrolyte have 80% mean crack percentage at 353 ppm whereas N and V3 (plated with lower organic concentration) have 40% mean crack percentage. In the case of Innolot solder joints after 2000 cycles, V9 solder joints exhibited the higher crack percentages at all strain amplitudes and was the only plating variant which exhibited 100% crack. All the other plating variants (V3, V27, N) performed in a similar way at their respective strain

amplitude levels. V9 contains larger amount of organic additives in the electrolyte during matte-Sn electroplating process and the plating was done at lower temperature (17 °C) compared to nominal temperature (22°C). The higher concentration of organic additives is added to reduce the grain size of deposited Sn but the organic additives contaminate the Sn deposit at the grain boundaries [9]. Even though V27 contained higher organic additives during plating, the higher temperature could have assisted in the desorption of the organic molecules which resulted overall lower organic content in the plating. From these results, the combination of high organic additives in the electrolyte and lower temperature shows the worst reliability performance in both SAC305 and Innolot solder joints.

# SEM and EDS investigation

Different regions of the gull wing developed IMC phases with different compositions (figure 6a) depending on their distance from the Cu-PCB pad irrespective of the solder alloy (SAC305 or Innolot) and the plating variant (V3, V9, V27, N). The top surface of the gull wing shows the diffusion of the Ni underlayer to form Ni-Sn IMC phase as seen in the Ni-map in figure 6b. EDS point scan revealed the composition of the Ni to be 40±0.3 at.% and that of Sn to be 59±0.4 at.% which corresponds to the Ni<sub>2</sub>Sn. IMC phase. Here, the diffusion of Ni can be seen which acted as diffusion barrier for Cu (refer Cu map in figure 6b). The presence of Ag-Sn IMC precipitates from the solder alloy is also seen by the Ag map in figure 6b. On contrary, the bottom surface of the gull wing showed limited diffusion of Ni underlayer as seen in the Ni map in figure 6c which led to the formation of (Cu,Ni), Sn, IMC phase as seen by the Cu and Sn map in figure 6c. The line scan reveals the presence of Ni-gradient within the (Cu,Ni), Sn<sub>5</sub> phase. Usually, the expected phase to form between Ni and Sn at solder joint relevant temperatures (<300°C) is Ni<sub>3</sub>Sn<sub>4</sub> as seen on the top surface of the pin [10], [11]. The formation of (Cu,Ni), Sn, IMC on a Ni surface on the bottom surface of the gull wing is due to the presence of excess Cu that diffused from the Cu surface on PCB side during reflow soldering and subsequently during thermomechanical cycling [12], [13]. Thermodynamically, the growth of (Cu,Ni) Sn<sub>z</sub> is possible when the Cu content in the Sn exceeds 8 at% locally [12]. But the SAC305/Innolot solder alloy contains maximum of 0.5 at% Cu. Hence the excess Cu must come from the Cu on the PCB side. Moreover, the microstructure changes from  $(Cu,Ni)_{\epsilon}Sn_{\epsilon}$  to  $(Cu,Ni)_{\epsilon}Sn_{\epsilon} + Ni_{\epsilon}Sn_{\epsilon}$  to  $Ni_{\epsilon}Sn_{\epsilon}$  along the bottom surface of the gull wing as the distance increases from the Cu on the PCB side as shown in figure 6a. The local IMC composition depends on the Cu concentration close to the interface between Ni underlayer and Sn. This fits perfectly to the argument that Cu on the PCB side acts as the Cu reservoir leading to change in IMC composition. On the Cu-PCB side, two IMC phases, Cu<sub>2</sub>Sn<sub>2</sub> and Cu<sub>2</sub>Sn IMC phases are formed which can be seen from the Cu-map in figure 6d. The thickness of the Cu<sub>2</sub>Sn layer is thin in the standoff region (yellow box) compared to the region far from standoff due to the diffusion of Ni from the component side Ni from the Niunderlayer must have dissolved into the Sn solder during reflow soldering and segregated towards the PCB pad side leading to enhanced growth rate of Cu<sub>6</sub>Sn<sub>5</sub> phase and decreased the Cu<sub>3</sub>Sn growth rate [14].

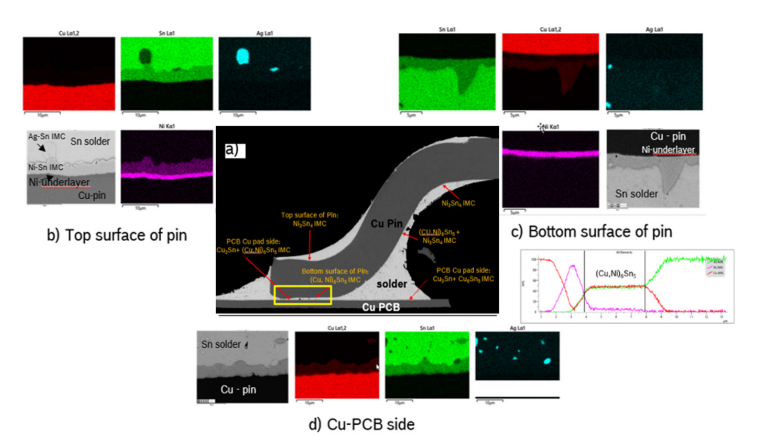
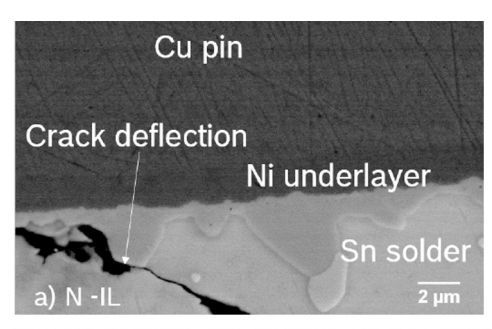


Figure 6: Elemental EDS mapping of Cu, Ni, Sn and Ag in V9-SAC gull wing pin solder joint after 2000 thermo-mechanical cycles. a) LFPAK gull wing with different IMC phases present in different regions, b) Top surface of the gull wing pin showing  $\mathrm{Ni_3Sn_4}$  phase c) Bottom surface of the gull wing pin showing  $(\mathrm{Cu_7Ni)_6Sn_5}$  phase with Nigradient as seen by the line scan and d) Cu PCB side showing growth of  $\mathrm{Cu_6Sn_5} + \mathrm{Cu_3Sn}$  phases. Yellow boxed region is the critical standoff region.

Even though crack initiations/shorter cracks have been observed from both meniscus sides (as seen in figure 2a) in components that have been subjected to lower strain levels, the crack reaches the IMC | Sn interface at the component side (yellow box zone) faster on the left meniscus due to the limited solder availability and further crack propagation characteristics are dependent on the (Cu,Ni) Sn | Sn interface on the component side as shown in figure 7. Table 3 provide the thickness, roughness and Ni content of the (Cu,Ni),Sn<sub>5</sub> IMC measured on component side. The almost flat (Cu,Ni), Sn. IMC morphology of V9 which has lower Ni content (3 at%) in the (Cu,Ni), Sn<sub>E</sub> IMC enables the crack to propagate without any obstruction as seen in figure 7b whereas in case of N which has higher Ni (10 at%) in (Cu,Ni) Sn, IMC and has rougher morphology, the crack is deflected from the IMC/ Sn interface towards the more ductile Sn as seen in figure 7a. The rougher interface increases the energy for crack propagation in comparison to a flatter IMC | Sn interface which attributes to lower crack percentages in solder joints which had N plating variant as opposed to the higher crack percentages in V9 for the same number of thermo-mechanical cycles. Thus, the electroplating parameters of matte-Sn influences the Ni-content and hence the morphology of the (Cu,Ni), Sn, IMC that forms on the Ni-underlayer on the component side. The standoff distances in this study were measured to have normal distribution (Avg: 22μm, standard deviation: ± 8μm) and no direct correlation were observed to the type of failure observed. The morphology of the (Cu,Ni), Sn, IMC in the standoff zone primarily determines the crack propagation characteristics for the standoff distances relevant in this study.



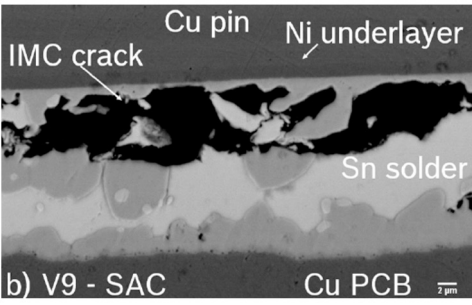


Figure 7: a) Crack deflected by the rough  $(Cu,Ni)_{\epsilon}Sn_{\epsilon}$  IMC in N-Innolot solder joint. b) IMC crack propagated through the  $(Cu,Ni)_{\epsilon}Sn_{\epsilon}$  IMC/solder interface in V9-SAC solder joint

Table 3: (Cu,Ni)<sub>6</sub>Sn<sub>5</sub> IMC thickness and roughness in the standoff region for plating variant-solder combination after 2000 cycles. The gradient of Ni in IMC is provided by measuring the Ni at. % at the middle of the IMC and close to the IMC/solder interface using EDS area scans. The standard deviations are provided in brackets.

Plating Variant	Solder	IMC thick- ness (µm)	IMC rough- ness (µm)	Ni at. % middle of IMC	Ni at. % close to IMC/ solder	Ni at. % gra- dient
V3	SAC	3.43	1.73	7.5 (1.2)	2.3 (1.1)	5.2
V9	SAC	3.65	0.78	3.4 (0.9)	<0.5 (0.5)	2.9
V27	SAC	3.56	1.2	7.2 (1.1)	0.9 (0.3)	2.3
N	SAC	4.23	2.23	10.5 (0.9)	3.2 (0.9)	7.3
V3	IL	2.34	1.43	5.6 (0.8)	1.3 (0.6)	4.3
V9	IL	2.23	0.34	2.7 (1.6)	1.2 (0.8)	1.5
V27	IL	3.23	0.43	4.4 (0.8)	2.1 (0.6)	2.3
N	IL	3.34	1.92	8.4 (0.6)	3.4 (1.2)	5

### **CONCLUSIONS**

The effect of matte-Sn electroplating parameters on the thermomechanical reliability has been studied and the following conclusions have been derived:

- 1. The combined effect of thermal and mechanical loads during thermo-mechanical cycling leads to early solder joint failure compared to pure thermal cycling. Minimum of 400 ppm of microstrain is required to visualize the effect of minor influencing factors such as matte-Sn electroplating parameters.
  - 2. Regardless of the electroplating conditions, Innolot has high

thermo-mechanical reliability than SAC305 solder alloy.

- 3. Electroplating parameters of matte-Sn have notable influence on the thermo-mechanical performance of both SAC and IL solder joints.
- 4. The electroplating parameters with high organic additives in the electrolyte and lower plating temperatures exhibits brittle failure through IMC crack mode.
- 5. Microstructural investigation suggests that the electroplating parameters affect the Ni content and morphology of the (Cu,Ni)<sub>6</sub>Sn<sub>5</sub> IMC which inturn influences the crack propagation path either deflecting to Sn or continuing via IMC|Sn interface.

#### **REFERENCES**

- [1] B. Vandevelde, M. Gonzalez, P. Limaye, P. Ratchev, and E. Beyne, "Thermal cycling reliability of SnAgCu and SnPb solder joints: A comparison for several IC-packages," Microelectronics Reliability, vol. 47, no. 2–3, pp. 259–265, Feb. 2007, doi: 10.1016/j. microrel.2006.09.034.
- [2] C. Shen et al., "Packaging Reliability Effect of ENIG and ENEPIG Surface Finishes in Board Level Thermal Test under Long-Term Aging and Cycling," Materials, vol. 10, no. 5, p. 451, Apr. 2017, doi: 10.3390/ma10050451.
- [3] P. Choudhury and S. Sarkar, "Development of lead-free alloys with ultra-high thermo-mechanical reliability," Proceedings of SMTA International, 2015.
- [4] H. Li, T. An, X. Bie, G. Shi, and F. Qin, "Thermal fatigue reliability analysis of PBGA with Sn63Pb37 solder joints," in 2016 17th International Conference on Electronic Packaging Technology (ICEPT), Wuhan: IEEE, Aug. 2016, pp. 1104–1107. doi: 10.1109/ICEPT.2016.7583318.
- [5] B. Torres-Montoya, D. Duffek, J. Mason, E. Corona, M. Chengalva, and M. Cavanaugh, "Effects of combined cyclic thermal and mechanical loading on fatigue of solder joints," in The Ninth Intersociety Conference on Thermal and Thermomechanical Phenomena in Electronic Systems (IEEE Cat. No.04CH37543), Las Vegas, NV, USA: IEEE, 2004, pp. 280–286. doi: 10.1109/ITHERM.2004.1318294.
- [6] U. Welzel, L. Lagarde, Y. Wang, F. Schempp, and R. B. GmbH, "Temperature Cycling with Bending to Reproduce Typical Product Loads", Proceedings of SMTA International, 2020.
- [7] I. Kim and S.-B. Lee, "Fatigue Life Evaluation of Leadfree Solder under Thermal and Mechanical Loads," in 2007 Proceedings 57th Electronic Components and Technology Conference, Sparks, NV, USA: IEEE, 2007, pp. 95–104. doi: 10.1109/ECTC.2007.373782.
- [8] Q. B. Tao, L. Benabou, K. L. Tan, J. M. Morelle, and F. B. Ouezdou, "Creep behavior of Innolot solder alloy using small lap-shear specimens," th Electronics Packaging Technology Conference, p. 6, 2015.
- [9] A. Sharma, S. Das, and K. Das, "Pulse Electroplating of Ultrafine Grained Tin Coating," in Electroplating of Nanostructures, M. Aliofkhazraei, Ed., InTech, 2015. doi: 10.5772/61255.
- [10] C. Ghosh, "Study on important diffusion parameters of binary Ni<sub>4</sub>Sn<sub>4</sub> phase," J Mater Sci: Mater Electron, vol. 24, no. 7, pp.

2558-2561, Jul. 2013, doi: 10.1007/s10854-013-1133-2.

- [11] C. Wang and J. Liu, "Effects of Sn thickness on morphology and evolution of Ni<sub>3</sub>Sn<sub>4</sub> grains formed between molten Sn and Ni substrate," Intermetallics, vol. 61, pp. 9–15, Jun. 2015, doi: 10.1016/j.intermet.2015.02.002.
- [12] T. Laurila, V. Vuorinen, and J. K. Kivilahti, "Interfacial reactions between lead-free solders and common base materials," Materials Science and Engineering: R: Reports, vol. 49, no. 1–2, pp. 1–60, Mar. 2005, doi: 10.1016/j.mser.2005.03.001.
- [13] A. Wierzbicka-Miernik, J. Wojewoda-Budka, K. Miernik, L. Litynska-Dobrzynska, and N. Schell, "Characteristics of intermetallic phases in Cu/(Sn,Ni) diffusion couples annealed at 220 °C," Journal of Alloys and Compounds, vol. 693, pp. 1102–1108, Feb. 2017, doi: 10.1016/j.jallcom.2016.09.147.
- [14] V. A. Baheti, S. Kashyap, P. Kumar, K. Chattopadhyay, and A. Paul, "Solid–state diffusion–controlled growth of the intermediate phases from room temperature to an elevated temperature in the Cu–Sn and the Ni–Sn systems," Journal of Alloys and Compounds, vol. 727, pp. 832–840, Dec. 2017, doi: 10.1016/j.jallcom.2017.08.178.